



LJMU Research Online

Subotic, I, Bodo, N and Levi, E

An EV Drive-Train With Integrated Fast Charging Capability

<http://researchonline.ljmu.ac.uk/id/eprint/2357/>

Article

Citation (please note it is advisable to refer to the publisher's version if you intend to cite from this work)

Subotic, I, Bodo, N and Levi, E (2015) An EV Drive-Train With Integrated Fast Charging Capability. IEEE TRANSACTIONS ON POWER ELECTRONICS, 31 (2). pp. 1461-1471. ISSN 0885-8993

LJMU has developed **LJMU Research Online** for users to access the research output of the University more effectively. Copyright © and Moral Rights for the papers on this site are retained by the individual authors and/or other copyright owners. Users may download and/or print one copy of any article(s) in LJMU Research Online to facilitate their private study or for non-commercial research. You may not engage in further distribution of the material or use it for any profit-making activities or any commercial gain.

The version presented here may differ from the published version or from the version of the record. Please see the repository URL above for details on accessing the published version and note that access may require a subscription.

For more information please contact researchonline@ljmu.ac.uk

<http://researchonline.ljmu.ac.uk/>

An EV Drive-Train With Integrated Fast Charging Capability

Ivan Subotic, *Student Member, IEEE*, Nandor Bodo, and Emil Levi, *Fellow, IEEE*

Abstract—This paper proposes a new class of on-board chargers for electric vehicles (EVs). Instead of being placed on-board as a separate unit, the three-phase (fast) chargers reutilize the existing components in EVs, which are already used for the propulsion. These are primarily the inverter and the machine, which however have to be multiphase (with more than three phases). The concept is valid for all multiphase propulsion drives with a prime number of phases higher than three and a single neutral point in motoring and is illustrated in detail for the five-phase inverter/five-phase machine configuration. During the charging mode, electromagnetic torque is not produced in the machine so that the rotor does not require mechanical locking. Hardware reconfiguration between propulsion and fast charging is required, but it is achieved with only two switches, which are the only two nonintegrated elements. The integrated topology is explained in this paper, together with the control scheme, and extension from five phases to higher phase numbers is illustrated using the seven-phase system as an example. Finally, the propulsion-mode operation with complete suppression of low-order harmonics, which map into the second plane, is achieved for the five-phase machine. Experimental verification of theoretical results and proposed control is provided for both charging and vehicle-to-grid mode of operation, as well as for propulsion.

Index Terms—Battery chargers, electric vehicles (EVs), five-phase machines, integrated on-board chargers.

I. INTRODUCTION

AN area of electric vehicles (EVs) that is recently receiving a lot of attention is charging. The main challenge is to provide an infrastructure that will be capable to withstand high charging demands that will inevitably be seen in the future, as a result of the increase in the number of EVs. A significant problem is that a high number of fast charging stations would have to be installed; considering the high cost of a typical modern dc charging station, this is not an easy task. One possible way of circumventing this problem is to equip vehicles with on-board chargers and develop an infrastructure with multiple access points to three-phase ac mains. This requires existence of on-board battery chargers.

Fast charging requires significant installed power of the battery charger. However, increasing the power rating of on-board chargers substantially is not viable, since it would load the vehicle with unacceptably high additional weight and would increase

the cost significantly. Fortunately, the power electronic components that are required for rectification of ac voltages and those that are used in EVs for propulsion are very similar; moreover, the two modes of operation are never encountered simultaneously. This has led to the idea of integrating the two functions more than 30 years ago [1] by using the same components. At present, integrated chargers are seen as one of the most important contestants for solving the mass charging problem, as they allow reduction of cost, weight, and required space in the vehicle.

Although there are numerous proposals for integration, as surveyed in [2]–[4], the vast majority are restricted to single-phase (slow) charging [5]–[11]. The main reason for this situation is that it is relatively easy to avoid electromagnetic torque production in the machine during the single-phase charging. However, single-phase charging is restricted by the capacity of the mains outlet and is always of low maximum power so that the charging process is inherently slow.

A review of the EV propulsion motor technology [12] shows that the majority of modern EVs use either induction or PM synchronous motor for propulsion, which are currently three-phase. The first fast integrated charger that found its place in industry is “Chameleon charger” [13], [14], which is at present commercially used in Renault ZOE. It utilizes a synchronous motor with excitation winding. However, for charging purposes, additional nonintegrated elements are required. The main nonintegrated component is an additional rectifier. Upon rectification, dc current is passed through the motor so that the stator winding now takes the role of filtering inductance. It appears that the charging configuration and operation rely on patents described in [15] and [16].

Due to the nature of the three-phase system, it seems that it is impossible to design a fully integrated charger without any additional nonintegrated components, when three-phase charging is required and a three-phase motor is used, while achieving the zero torque production. The closest one can get to this is either to use the system described above, where the machine is used to filter the charging current but an additional rectifier is required, or the solution of [17], in which the three-phase converter is integrated in the charging system and performs the role of the PWM controlled inverter/rectifier in the propulsion/charging modes. However, in the solution of [17], the motor is disconnected during charging using a special switch and additional filtering reactors are the additional nonintegrated components required. Finally, Hong *et al.* [18] utilizes a three-phase machine for the charging purposes but requires an additional nonintegrated charger.

However, the situation radically changes if the propulsion motor has more than three phases. In [19], a three-phase machine

Manuscript received October 24, 2014; revised February 18, 2015; accepted April 8, 2015. Date of publication April 20, 2015; date of current version September 29, 2015. The authors would like to acknowledge the Engineering and Physical Sciences Research Council (EPSRC) for supporting the “Vehicle Electrical Systems Integration (VESI)” project (EP/I038543/1). Recommended for publication by Associate Editor S. Williamson.

The authors are with the School of Engineering, Technology, and Maritime Operations, Liverpool John Moores University, Liverpool L3 3AF, U.K. (e-mail: i.subotic@2011.ljmu.ac.uk; n.bodo@2009.ljmu.ac.uk; e.levi@ljmu.ac.uk).

Color versions of one or more of the figures in this paper are available online at <http://ieeexplore.ieee.org>.

Digital Object Identifier 10.1109/TPEL.2015.2424592

TABLE I
QUANTITATIVE COMPARISON OF THREE-PHASE (FAST) CHARGING SOLUTIONS

Ref.	Fault-tolerance in propulsion mode	Number of machine phases	Number of converter legs	EMI filter would not influence the propulsion mode	Torque-free charging operation	Hardware reconfiguration not required	Galvanic isolation required
[19]	✓	3	6	✗	✓	✓	✗
[21]	✗	6	3	✗	✓	✗	✗
[23]	✓	9	9	✗	✓	✓	✗
[15]	✗	3	6	✓	✓	✓	✗
[24]	✓	6	6	✓	✓	✗	✓
Fig. 1	✓	5	5	✓	✓	✗	✗

is supplied from a triple H-bridge in the propulsion mode. The machine is three-phase, but of special construction, so that midpoints of the three individual phase windings are accessible (thus the machine is an equivalent of a symmetrical six-phase machine). These midpoints are used to connect terminals of the three-phase grid in charging mode. By simultaneous switching of pairs of inverter legs, connected to the same grid phase, the same current flow is achieved through two half-windings of the machine that belong to the same machine's phase. Since these two half-windings are in space opposition, they cancel each other's effect so that there is no field and consequently no torque production in the machine. The configuration has a great additional feature, namely it does not require any hardware reconfiguration between the propulsion and the charging mode. It is currently being considered by Valeo for the use in future EVs [20].

Another solution that employs a six-phase machine is described in [21]. During the charging mode, it operates using the principle similar to the one of [19]. The important difference is that it requires a hardware reconfiguration, since a three-phase inverter is used (unlike in [19], where a six-phase inverter is employed) in both propulsion and charging. An interesting isolated solution, also based on a six-phase machine, is presented in [22]. However, a torque is produced during the charging process.

An alternative configuration that does not require any hardware reconfiguration in order to achieve charging is presented in [23]. It incorporates a nine-phase machine and a nine-phase inverter into the charging process. In the propulsion mode, it operates with three isolated neutral points, while during the charging process those neutral points are directly connected to the three terminals of the three-phase grid. The control achieves the same current flow in all machine phases that are connected to the same grid phase. In this manner, the field is cancelled within each of the three machine's three-phase sets. Hence, the excitation in the first (torque/flux producing) plane is identically equal to zero, no electromagnetic torque is produced during charging, and no hardware reconfiguration is required. When compared to the solution of [19], three rather than two three-phase inverters are required; however, excellent fault tolerance exists in the propulsion mode so that realization of the limp-home mode is rather simple.

Two further fast charging solutions with six-phase machines, this time of isolated type and using a six-phase converter, are presented in [24]. One applies to a symmetrical six-phase machine

(as in [19]), while the other is valid for an asymmetrical six-phase machine. The configurations employ the principle of phase transposition [25] in order to avoid torque production during the charging process.

A common characteristic of the solutions with symmetrical six-phase machine [19], with symmetrical or asymmetrical nine-phase machine [23], and with asymmetrical six-phase machine [24] is that the first (flux/torque producing) plane is left completely without excitation during charging. Hence, currents of the machine fully map into the other nonflux/torque producing planes [26]. However, another possibility exists. It is to divert machine currents in such a way that only one axis current in the first plane flows so that a pulsating field exists during charging. Such a solution is given for the symmetrical six-phase topology in [24]. The idea is here generalized to multiphase systems with a prime number of phases and a single neutral point.

A quantitative comparison of some of the existing solutions is given in Table I. This paper proposes a new integrated charger concept, based on the integration of a multiphase machine with a prime phase number higher than three and a single neutral point, and a multiphase inverter. The principle relies on the production of the pulsating field in the first plane and is developed in detail for the five-phase topology. Extension to higher prime phase number is illustrated using the seven-phase system as an example.

This paper is organized as follows. The charging topology is introduced and its operating principles explained at a theoretical level, using the five-phase topology, in Section II. Extension of the principle to higher prime phase numbers, assuming single neutral point in the propulsion mode, is presented in Section III. Control algorithms are then described in Section IV and experimental results are reported in Section V for the five-phase system to validate the concept and the theoretical considerations. Experimental verification is provided for both charging and vehicle-to-grid (V2G) modes, as well as for the propulsion mode of operation. Section VI concludes this paper.

II. TOPOLOGY AND OPERATING PRINCIPLES

The proposed topology is depicted in Fig. 1 for the five-phase system. In the propulsion mode, switches S_1 and S_2 are both closed. The drive has a single neutral point, as the case is typically with all multiphase machines with a prime phase number [26], [27]. Switch S_1 carries current of the machine's phase

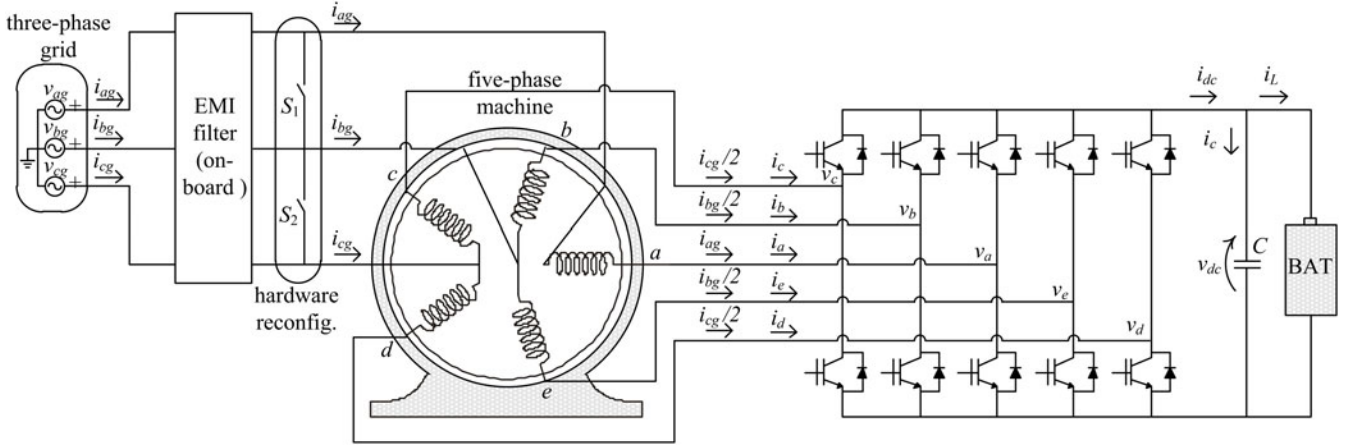


Fig. 1. Topology of the proposed integrated five-phase charging system.

a , while S_2 carries sum of the currents of machine's phases c and d . A five-phase system in the propulsion mode appears to represent a good tradeoff between two mutually opposing requirements for vehicular applications, enhanced fault tolerance, and the low complexity of the system. Fault-tolerant operation with multiphase machines is based on the fact that only two independently controllable currents are required for independent flux and torque control so that when there are more than three phases, there exist additional degrees of freedom which can be used to achieve the postfault operation [26]. The propulsion mode of operation of a five-phase machine during a fault has been covered extensively in the past (e.g., [28], [29]) and is beyond the scope of this paper. The five-phase machine used later on to experimentally prove the viability of the concept of Fig. 1 is of induction type; however, the concept is equally applicable to five-phase synchronous machines as well.

An EMI filter will normally be used in the charging mode. Since its three-phase connections are short-circuited, it does not influence the propulsion mode, and it can remain attached without any interference in this mode of operation. It should be noted that this is the only configuration that has this advantage and does not accomplish it by placing the EMI filter on the grid side of an additional nonintegrated element (see Table I). The nonintegrated element is a rectifier in [15], it is a set of filtering reactances in [17], while it is an isolation transformer in [24]. On the other hand, if charging is considered, all the other solutions in Table I have either the machine phase number or the inverter leg number equal to at least 6. Thus, the five-phase system is the only fully integrated fast charging system which enables reduction of this phase number below 6.

The topology in Fig. 1 is shown without a dc–dc converter. However, it should be noted that if the battery voltage cannot reach the peak of the grid line-to-line voltage, a bidirectional dc–dc converter should be included between the battery and the five-phase converter. Whether or not a dc–dc converter is used has no impact on the charging principle and control; thus, it is not considered further on.

For the three-phase charging, both switches S_1 and S_2 have to be opened. This connects grid phase a to an open terminal

of machine phase a , grid phase b is connected to a parallel connection of machine phases b and e , while grid phase c is applied to the parallel connection of machine phases c and d (see Fig. 1). Inverter legs that supply machine phases connected to the same grid phase are controlled using the same switching signals. Thus, there are only three gating signals. The first one goes to the inverter leg of phase a , the second one to the inverter legs connected to phases b and e , and the third one to legs supplying phases c and d .

One very important aspect of integrated chargers is whether electromagnetic torque gets produced in the machine during the charging mode. Machine's behavior can be easily assessed in the charging mode of operation by using the decoupling transformation matrix and examining the mapping of the currents into the planes of the five-phase system. The decoupling matrix is available in [26]; if represented in space vector form (symbol \underline{f} denotes current or voltage), it is governed with

$$\begin{aligned}\underline{f}_{\alpha\beta} &= f_{\alpha} + jf_{\beta} \\ &= \sqrt{2/5} (f_a + \underline{a}f_b + \underline{a}^2f_c + \underline{a}^3f_d + \underline{a}^4f_e) \\ \underline{f}_{xy} &= f_x + jf_y \\ &= \sqrt{2/5} (f_a + \underline{a}^2f_b + \underline{a}^4f_c + \underline{a}^6f_d + \underline{a}^8f_e)\end{aligned}\quad (1)$$

where $\underline{a} = \exp(j\delta) = \cos\delta + j\sin\delta$ and $\delta = 2\pi/5$. Indices α, β denote the flux/torque producing plane, and indices x, y stand for the nonflux/torque producing plane(s).

In a three-phase system, the grid currents are governed with

$$i_{kg} = \sqrt{2}I \cos(\omega t - l2\pi/3), \quad l = 0, 1, 2, \quad k = a, b, c. \quad (2)$$

From Fig. 1, it can be seen that the relationship between grid and machine currents is

$$i_a = i_{ag}, \quad i_b = i_e = i_{bg}/2, \quad i_c = i_d = i_{cg}/2. \quad (3)$$

The substitution of (2) and (3) into (1) leads to the following two space vectors:

$$\underline{i}_{\alpha\beta} = I \cdot \sqrt{2} \cos(\omega t - 0.659) \quad (4)$$

$$\underline{i}_{xy} = I \cdot \sqrt{2} \cos(\omega t + 0.659). \quad (5)$$

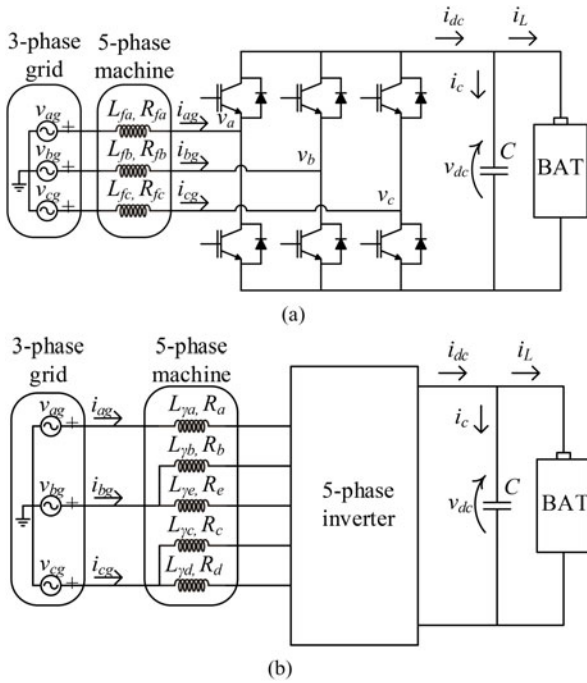


Fig. 2. (a) Equivalent scheme of the configuration of Fig. 1 during the fast (three-phase) charging operation and (b) equivalent circuit showing machine's phase connections to the grid phases.

Obviously, there is excitation in the first (torque producing) plane. However, only the α -component exists, while β -component is zero. This leads to the production of a pulsating field in the machine, which is not capable of creating a starting torque. Consequently, in this mode of operation, the machine's rotor will be kept naturally at standstill, without the need for any mechanical brake. The pulsating field in the machine will cause iron losses in both stator and rotor of the machine. However, while the former is always inevitable if the machine plays the role of filtering inductances, the latter is unavoidable when rotor bars are to be utilized in order to increase the equivalent filtering inductance, as the case is here. The issue is further discussed in Section IV.

Equivalent circuit representation of the system in charging mode is shown in Fig. 2(a), where filter parameters (R and L) are not equal for all the three phases; these are in essence equivalent machine parameters as seen from the grid side and relate to the way in which the machine phases are connected to the grid phases [see Fig. 2 (b)].

III. EXTENSION OF THE PRINCIPLE TO HIGHER PHASE NUMBERS

The principle of keeping the β -component at zero and exciting only the α -component in the flux/torque producing plane can be applied to all the other systems with a prime number of phases. Two different approaches can be followed when there are seven phases or more. In the first one, phase a of the grid will always get connected to the phase a of the machine, and this is simultaneously α axis. Phases that produce β -components

of equal values but of opposite sign should be connected to the same grid phase. This comes down to connecting to the same grid phase (say, phase b), two phases of the machine at spatial positions $\delta = 2\pi/n$ and $(2\pi - \delta)$, and those at 2δ and $(2\pi - 2\delta)$ to phase c . This assures that they cancel each other's β -component of the field, and only the α -component remains. Obviously, when the number of phases exceeds seven, there is more than one possibility of machine phase selection for parallel connection to the given grid phases b and c . The drawback of this method is that as the phase number increases, charging mode power becomes smaller and smaller part of the motor propulsion mode power.

In the described approach, only five phases of the machine would be used regardless of the machine's phase number. An alternative way is to always involve all machine phases in the charging process, the advantages being that only two switches will always be required for hardware reconfiguration (regardless of the machine's phase number) and that the charging power will be closer to the propulsion rated power. The principle of β -component cancellation still has to be used. Hence in, say, a seven-phase system, one could connect machine phases a, b , and g to grid phase a , phases c and f to grid phase b , and phases d and e to grid phase c . This is illustrated next.

Decoupling transformation matrix of a seven-phase system can be given in complex space vector form with

$$\begin{aligned} \underline{f}_{\alpha\beta} &= \sqrt{2/7} (f_a + \underline{a}f_b + \underline{a}^2f_c + \underline{a}^3f_d \\ &\quad + \underline{a}^4f_e + \underline{a}^5f_f + \underline{a}^6f_g) \\ \underline{f}_{-x_1y_1} &= \sqrt{2/7} (f_a + \underline{a}^2f_b + \underline{a}^4f_c \\ &\quad + \underline{a}^6f_d + \underline{a}^8f_e + \underline{a}^{10}f_f + \underline{a}^{12}f_g) \\ \underline{f}_{-x_2y_2} &= \sqrt{2/7} (f_a + \underline{a}^3f_b + \underline{a}^6f_c \\ &\quad + \underline{a}^9f_d + \underline{a}^{12}f_e + \underline{a}f_f + \underline{a}^4f_g) \end{aligned} \quad (6)$$

where $\underline{a} = \exp(j\delta) = \cos \delta + j \sin \delta$ and $\delta = 2\pi/7$. Indices α, β denote the flux/torque producing plane, and indices x_1, y_1, x_2, y_2 stand for the two nonflux/torque producing planes.

Grid currents are again given with (2) and, according to the described principle of machine phase selection for paralleling to a given grid phase, their relations with machine phase currents are the following:

$$i_a = i_b = i_g = i_{ag}/3, \quad i_c = i_f = i_{bg}/2, \quad i_d = i_e = i_{cg}/2. \quad (7)$$

Subsequent substitution of (7) and (2) into (6) leads to the following excitations in the three planes:

$$\underline{i}_{\alpha\beta} = 1.0858 \cdot I \cdot \cos(\omega t - 0.4214) \quad (8)$$

$$\underline{i}_{x_1y_1} = 1.0275 \cdot I \cdot \cos(\omega t + 1.3304) \quad (9)$$

$$\underline{i}_{x_2y_2} = 0.6571 \cdot I \cdot \cos(\omega t - 2.1390). \quad (10)$$

Clearly, the excitation in the torque producing plane is again only in the direction of the α -axis. Since the β -component is kept at zero, the field will be again pulsating and, hence, incapable of producing any starting torque. Again, the machine rotor will not

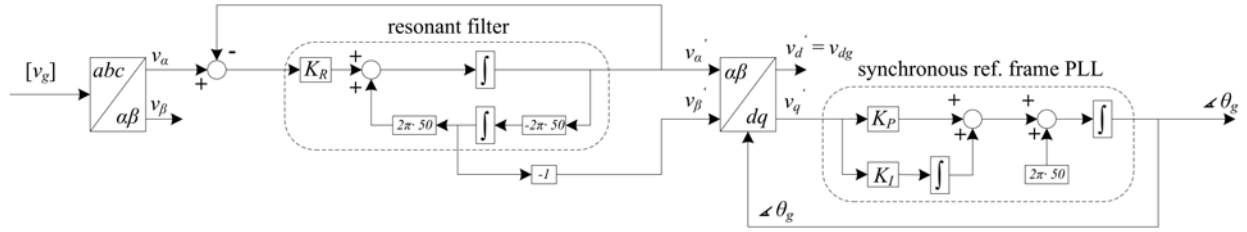


Fig. 3. PLL algorithm.

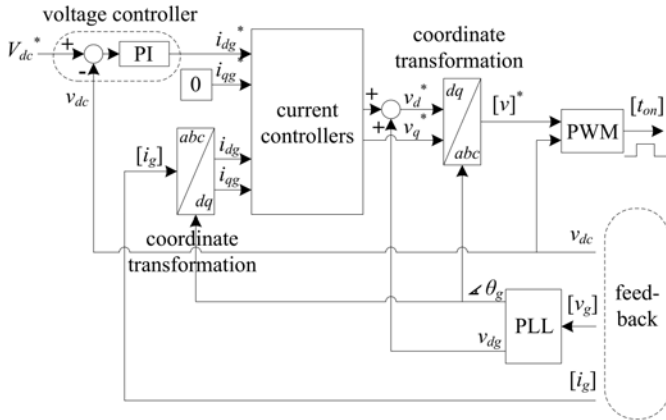


Fig. 4. Control algorithm for the charging configuration.

rotate so that it does not have to be mechanically locked during the charging or V2G process.

IV. CONTROL

A. Charging

It follows from Section II that the five-phase machine will not rotate during the three-phase charging process. Its equivalent scheme representation is hence facilitated since the machine can be represented as a simple set of passive components, as shown in Fig. 2(a). The connection arrangement between the grid and the machine is shown in Fig. 2(b). This section considers the control of the system in the charging mode. In some ways, the situation is similar with control of the configurations elaborated in [23] and [24]. However, for the sake of completeness, full control scheme is described here.

The configuration requires measurements of grid voltages, grid currents, and dc-bus voltage. It should be noted that additional current sensors, above those already required for the propulsion mode, are not needed since the grid currents can be obtained from machine currents.

In order to meet grid standards and regulations regarding unity power factor operation, voltage-oriented control (VOC) is utilized as the main control algorithm. Therefore, knowing the grid position is obligatory, and this is a logical first step. This information can be obtained from a phase-locked loop (PLL). In order to improve the response for distorted grids, the PLL shown in Fig. 3 is utilized.

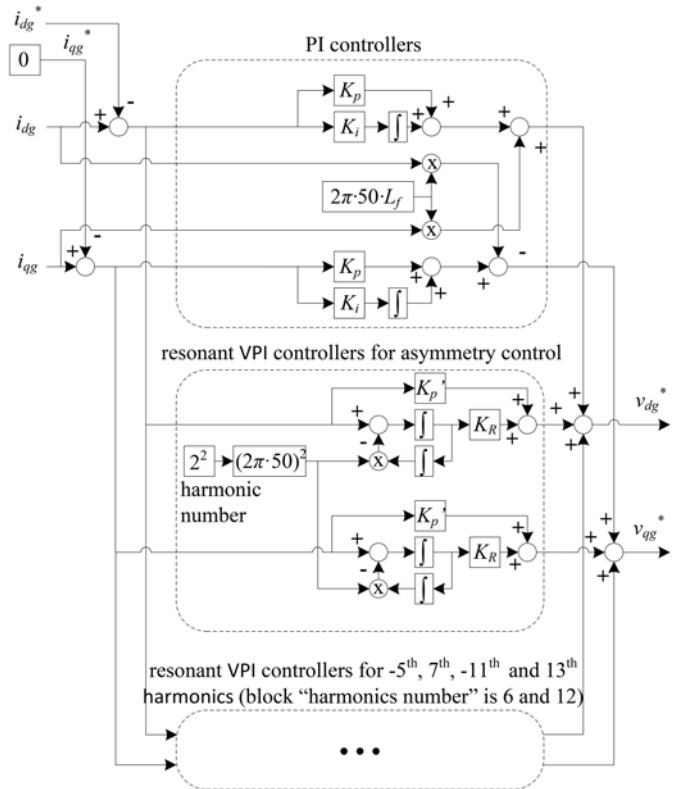


Fig. 5. Current controllers for the configuration shown in Fig. 2(a).

The control has to achieve unity power factor. In order to observe phase deviation from it, it is beneficial to transform grid currents into a rotating reference frame that is orientated according to the grid voltage. For this reason, VOC is used as a control algorithm (see Fig. 4). Grid currents are initially transformed using a decoupling transformation, and then into a synchronously rotating (dq) reference frame, utilizing the information on the grid position obtained from the PLL. Both transformations are in Fig. 4 represented with a single block labeled “coordinate transformation.” Now, the d -component is the grid-current component that is in phase with the grid voltage, and this is the component that can be used for energy transfer. The q -component represents grid current that is shifted from the d -component of the grid voltage by 90° ; thus, it should be kept at zero, at all times.

While the reference for the q -component is, naturally, zero, there are two manners of obtaining the reference for the d -component. If charging with constant current is required (CC

mode—usually at the beginning of charging process), the reference for the d -component should be obtained as the output of a battery charging current controller. However, close to the end of the charging process, the battery needs to be charged with a constant voltage (known as CV mode). Here the reference should be obtained from a dc bus voltage controller, which is represented as an outer control loop in Fig. 4.

When the current reference is obtained in one of the two ways described above, it enters the “current controllers” block in Fig. 4, which is shown separately in Fig. 5. The reference current components are getting subtracted from the real values. The reason for this reverse sign is the fact that higher converter voltages lead to a decrease in current, while the lower ones increase it. Since both actual and the reference component are dc values, their difference can be controlled with PI controller that is shown at the top of Fig. 5. This is sufficient for the fundamental control in symmetrical systems.

However, from Fig. 2, it can be seen that equivalent machine parameters are not the same with respect to the grid phases. If only fundamental component rotating in the synchronous direction is controlled, in stationary state, the output of the VSI is a vector that rotates in the synchronous direction and that has a fixed amplitude. Since the grid voltage is also a vector with fixed amplitude rotating in the synchronous direction, their difference is a vector with fixed amplitude rotating in the synchronous direction as well. Now, this difference is in essence the voltage that is applied to the filter (i.e., machine). Since the filter does not have the same impedance in all three phases, and considering that the voltage that is applied to all three phases is of the same amplitude, the currents flowing through the three phases will have different amplitudes. According to the theory of symmetrical components, this leads to a fundamental component that rotates in the antisynchronous direction and is seen from the dq reference frame as -2 nd harmonic (harmonic with frequency two times higher than fundamental, and that rotates in the direction that is opposite to synchronous). In order to achieve the same current rms values in all three phases, it is necessary to eliminate this harmonic. This can be done with vector proportional-integral (VPI) resonant controllers tuned for the cancellation of the second harmonic (middle part of Fig. 5).

The asymmetry in the machine’s equivalent scheme for the charging mode has two reasons. The first one is that phase a of the grid is connected to a single machine’s phase, while phases b and c are each connected to a parallel connection of two machine phases. Grid phase b is connected to machine phases b and e , while grid phase c is connected to machine phases c and d [see Fig. 2(b)]. Since machine phases that are connected to the same grid phase are connected in parallel to each other, their equivalent impedance is two times lower than the impedance of a single machine phase.

The second reason is the rotor influence. Namely, when a pulsating field enters the rotor, it induces currents in it (assuming that the motor is an induction machine, as the case is here) so that the rotor parameters start to play a role in the system. As field that stator produces pulsates, it causes only a pulsating field in the rotor. Therefore, induced currents in the rotor will create flux in a single direction only. Similarly, as the stator influences

rotor currents, the rotor currents also influence stator. However, since the rotor field pulsates, stator parts that are spatially shifted from the direction of pulsation by 90° will not see any influence of the rotor. On the other hand, stator parts that lay on the direction of the pulsation feel the whole impact of the rotor field. Therefore, the influence is higher on phases that are shifted from the direction of the pulsation by a smaller angle. Thus, machine’s phase a is influenced the most, since it lays on the direction of the pulsating field. On the other hand, machine phases c and d are shifted by 36° from the pulsating field direction. Therefore, the influence of rotor on them is smaller than on the phase a . Finally, the influence is the least on machine phases b and e as they are shifted from the direction of the pulsating field by 72° . Hence, the equivalent parameters of the grid phase b are increased the least, since they include parallel connection of machine phases b and e ; thus, this grid phase will have the lowest equivalent impedance. Naturally, the grid phase a will see the highest parameter values.

Finally, odd low-order harmonics, introduced by the inverter dead time, should also be compensated. In three-phase systems, these are predominantly the -5 th, 7 th, -11 th, and 13 th (minus sign denotes the antisynchronous direction of rotation). From the dq reference frame, these harmonics are seen as the -6 th, 6 th, -12 th, and 12 th harmonic, respectively. Both the -6 th and 6 th harmonic (as seen from the dq reference frame) can be conveniently controlled with a single VPI resonant controller in each axis that is tuned at the 6 th harmonic. Similarly, the -12 th and 12 th harmonics can be controlled with a single VPI controller in each axis that is now tuned for the 12 th harmonic. These controllers are exactly the same as the one for asymmetry control. The only difference lies in the block “harmonic number” which should instead of value 2 have values 6 and 12 , respectively.

Output of current controllers is summed with the d -component of the grid voltage. This is done to prevent high currents at the beginning of the charging process. Now, the sum is the reference for the dq components of the inverter voltage. When inverse rotational and inverse decoupling transformations are applied to them, references for inverter phase voltages are obtained. These enter PWM block which uses carrier-based modulation strategy with zero-sequence injection.

It should be noted that this control algorithm can be used unchanged for V2G operation. The only requirement is that a minus sign should be placed in front of the reference for the grid-current component i_{dg}^* .

B. Propulsion

As already stated, the propulsion mode of operation is well known for five-phase machines. Indirect rotor-field-oriented control, available in [26] and [27], is applied here with some modifications. In order to decrease computational time and improve harmonics control, different current controllers (compared to [27]), as shown in Fig. 6, are used in the second (xy) plane. The controllers are based on the idea that is presented in [30] for the case of an asymmetrical six-phase machine. The dominant harmonics that map into this plane are the 7 th and the -3 rd. In [27], current components of the xy plane are transformed and

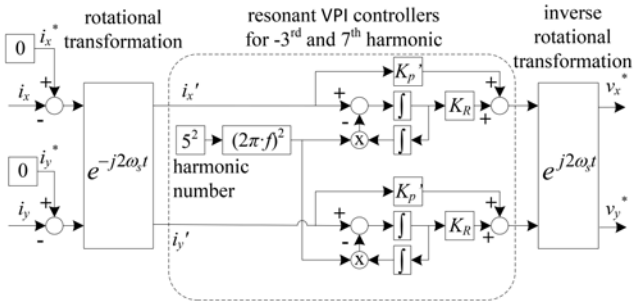
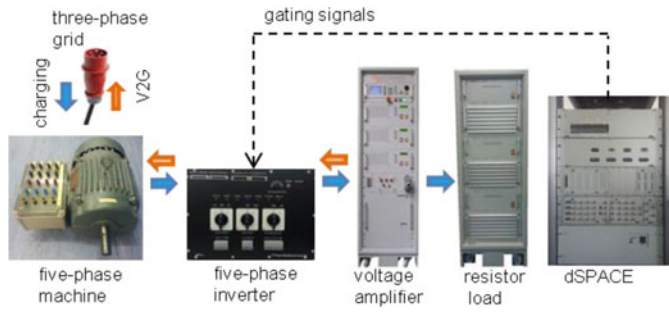
Fig. 6. Current controllers for x - and y -component in the propulsion mode.

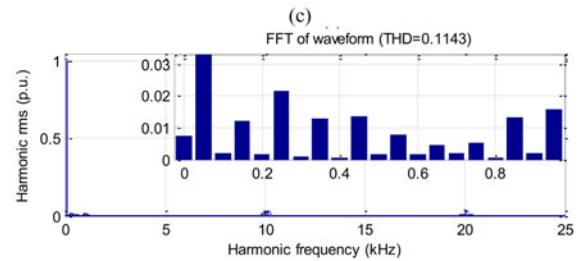
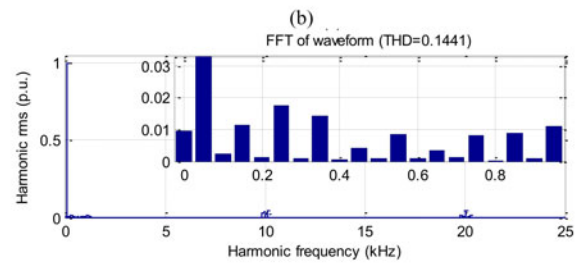
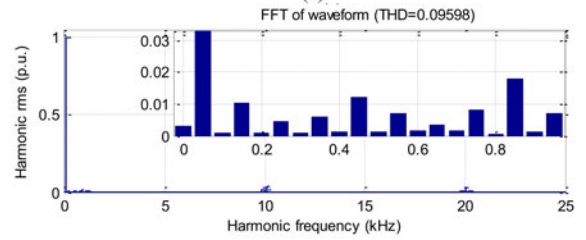
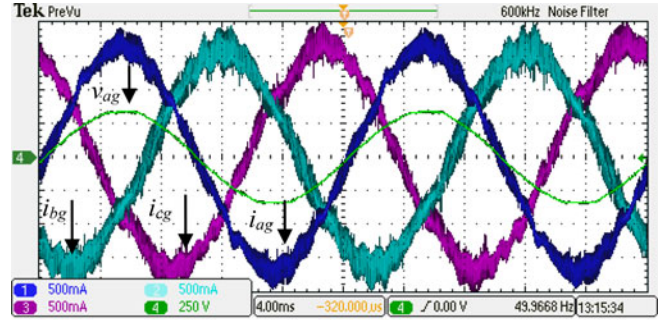
Fig. 7. Experimental rig.

subsequently controlled in the synchronous reference frame (i.e., the same frame used for dq current control). Here, a reference frame that rotates at twice the synchronous speed is selected for xy current components. This leads to the 7th and -3 rd harmonic (as seen from the stationary reference frame) appearing as the 5th and -5 th harmonic in the selected reference frame that rotates at twice the synchronous speed. Hence, both harmonics can be conveniently controlled by a single VPI controller placed in each axis, as illustrated in Fig. 6. Using the same idea, PI control of dq current components is enhanced with a VPI controller in the first plane to eliminate the -9 th and the 11th harmonics.

As already mentioned, the EMI filter that normally exists does not interfere with the propulsion mode. Thus, from the control perspective, its existence can be neglected.

V. EXPERIMENTAL RESULTS

Experiments are performed to validate the theoretical results of Section II and control schemes described in Section IV. Experimental rig is shown in Fig. 7, and data are given in appendix. The grid is three-phase, 415 V, 50 Hz. An amplifier “Spitzenberger & Spies” is used to emulate a battery and, therefore, dc–dc converter is not utilized. The amplifier has a maximum sinking power of 4 kW. Although this limits the charging power that can be achieved with the experimental rig, it by no means represents the power limit of the topology. A resistor of 0.5Ω is used to emulate battery’s internal resistance and is placed between the amplifier and the inverter. The converter operates at 10 kHz, with asymmetrical PWM; the control frequency is thus 20 kHz. Converter dead time is $6 \mu\text{s}$. Carrier-based modulation strategy with zero-sequence injection is utilized. Charging, V2G, and propulsion mode are evaluated in the next three sections.

Fig. 8. (a) Grid-phase voltage v_{ag} , grid currents i_{ag} , i_{bg} , i_{cg} . (b) Spectrum of grid current i_{ag} . (c) Spectrum of grid current i_{bg} . (d) Spectrum of grid current i_{cg} .

A. Charging Mode

Fast (three-phase) charging is assessed first. In the experiment, the EMI filter is not used so that all the filtering is performed by machine windings. Reference for the grid d current component is set to 2 A; this corresponds to the grid-current rms value of 1.15 A, since power invariant decoupling transformation is used. It should be noted that the reference could be also obtained from a battery current controller to demonstrate the CC mode, or from voltage controller to demonstrate the CV mode. Since this is not the focus here, a fixed value is chosen. The dc bus voltage is 720 V.

Grid-phase voltage v_{ag} and three grid currents are shown in Fig. 8(a). Unity power factor operation is obvious. It can be noticed that grid-current ripple is not the same, and is the highest in grid phase b . This is due to unequal equivalent scheme

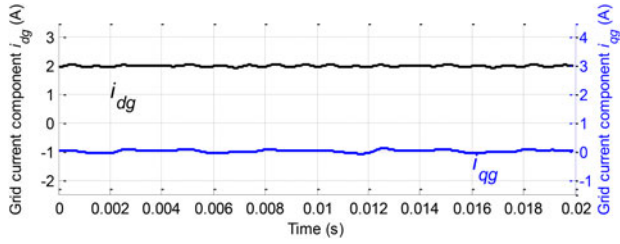


Fig. 9. Grid-current components i_{dg} and i_{qg} .

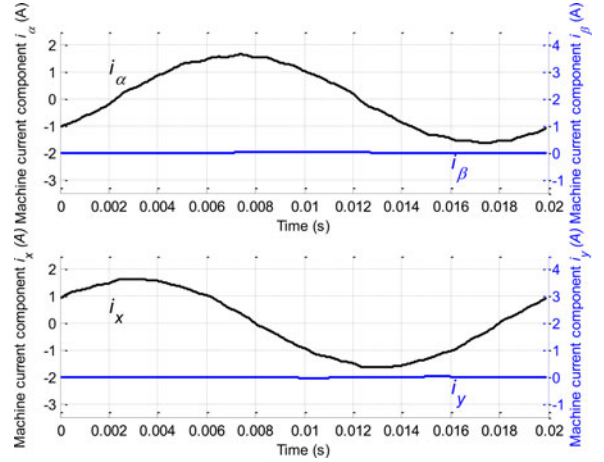


Fig. 11. Machine current components in the first (α/β) and the second plane (xy).

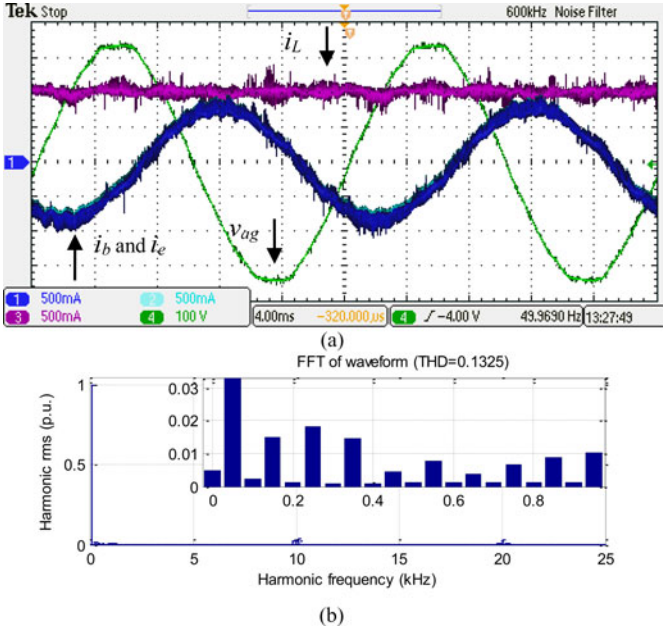


Fig. 10. (a) Grid-phase voltage v_{ag} , machine currents i_b , and i_e , battery charging current i_L . (b) Spectrum of machine current i_b .

parameters for this mode of operation, as elaborated in Section IV. However, although parameter asymmetry exists, it can be seen that grid currents have the same amplitudes, which verifies the “asymmetry control” block from Fig. 5. The spectra of grid currents i_{ag} , i_{bg} , and i_{cg} are shown in Fig. 8(b), (c), and (d), respectively, and they show good current quality. However, it can be seen that the THD is the highest in phase b , as it has the lowest equivalent impedance.

Grid-current components are shown in Fig. 9. The q -component is kept at zero, while the d -component follows its reference without a steady-state error. It can be seen that it does not contain the second harmonic, which again validates the asymmetry control part from Fig. 5.

Machine currents i_b and i_e are shown in Fig. 10(a), together with the traces of the grid-phase voltage v_{ag} and battery charging current i_L . These two currents are practically identical; since the traces in Fig. 10(a) are overlapped, the two currents appear as a single trace. Spectrum of one of these two currents is shown in Fig. 10(b). If compared to Fig. 8(c), the similarity is obvious. This is to be expected, since these two machine currents constitute the grid current i_{bg} .

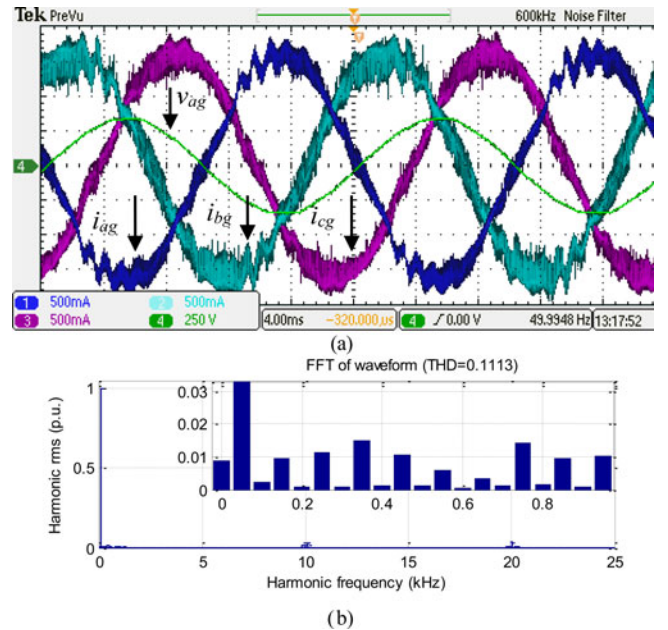


Fig. 12. (a) Grid-phase voltage v_{ag} , grid currents i_{ag} , i_{bg} , i_{cg} . (b) Spectrum of grid current i_{cg} .

Machine current components are shown in Fig. 11. In the torque producing (α/β) plane only α -component is generated. Thus, the field is pulsating, and the starting torque cannot be produced. The xy plane also has only one component excited and it is in the direction of the x -axis, which is in accordance with (5).

B. V2G Mode

V2G mode is obtained by setting the reference to $i_d^* = -2$ A. Grid-phase voltage v_{ag} and three grid currents are shown in Fig. 12(a) for this mode of operation. Grid current i_{ag} is in phase opposition with the voltage, thus unity power factor is again achieved. The currents again have the same amplitudes. The spectrum of the current i_{cg} is shown in Fig. 12(b).

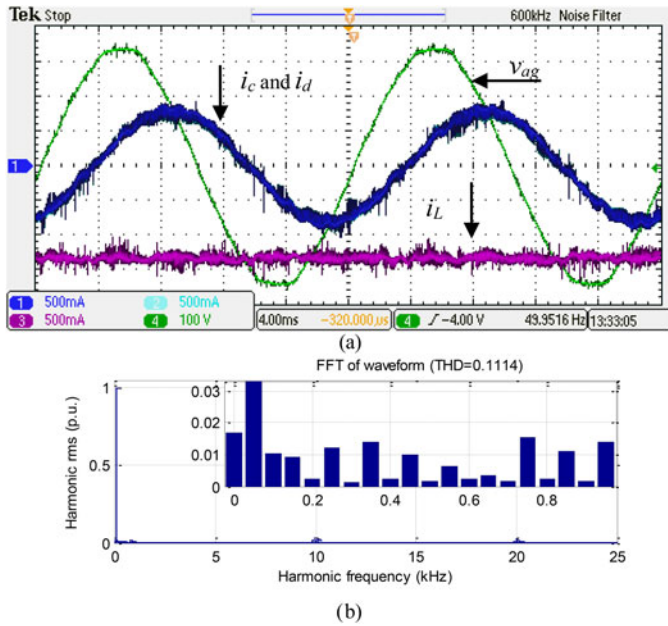


Fig. 13. (a) Grid-phase voltage v_{ag} , machine currents i_c , and i_d , battery charging current i_L . (b) Spectrum of machine current i_c .

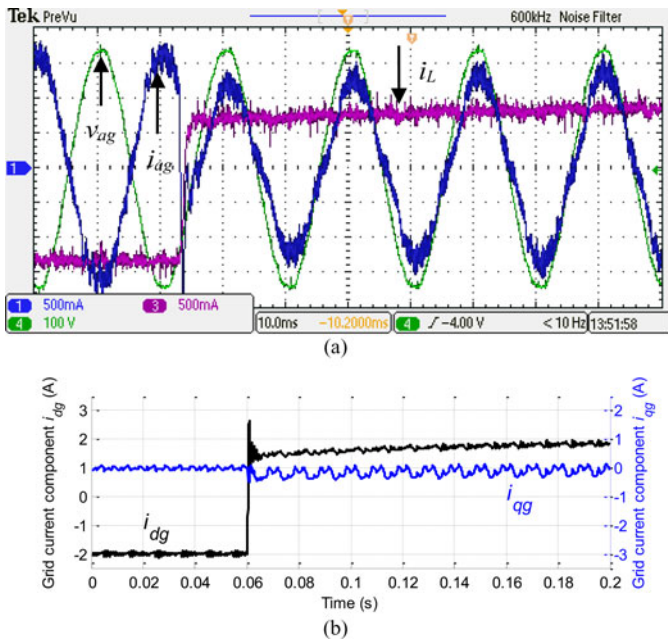


Fig. 14. (a) Grid-phase voltage v_{ag} , grid current i_{ag} , and battery charging current i_L . (b) Grid-current components i_{dg} and i_{qg} .

Machine currents i_c and i_d , which constitute the grid current i_{cg} , are shown in Fig. 13(a), together with the grid-phase voltage v_{ag} and battery charging current i_L . As the case was with machine currents i_b and i_e in Fig. 10, these two currents in essence appear as a single trace, since they are practically identical. Spectrum of one of the two is shown in Fig. 13(b) and it is similar to Fig. 12(b). Battery charging current is, like in the charging mode, a dc quantity. However, if compared to Fig. 10(a), it can be seen that it has a higher absolute value. This

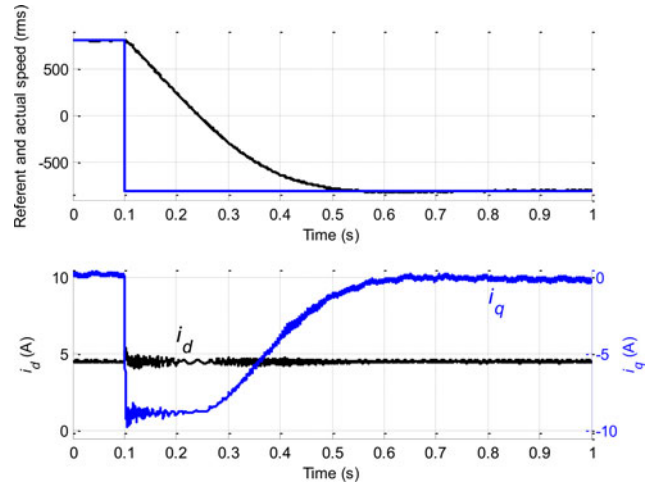


Fig. 15. Reversal transient from 800 to -800 r/min: the speed reference and actual speed (upper traces), and machine current components i_d and i_q (lower traces).

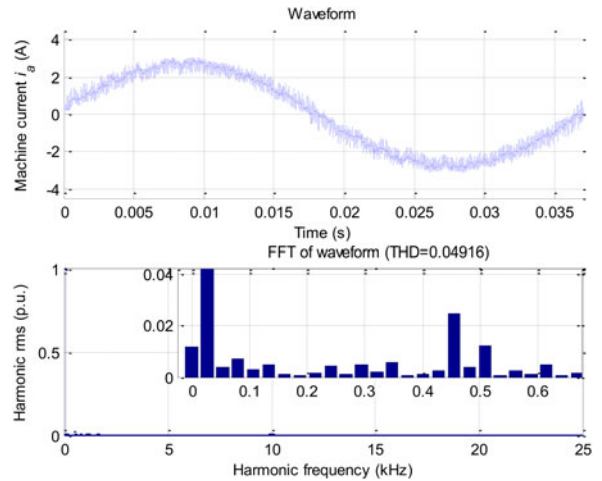


Fig. 16. Machine current i_a and its spectrum during a steady-state operation at a speed of 800 r/min.

is so because in the V2G mode, battery power covers losses in addition to the power that is injected into the grid. Unlike this, in the charging mode, the battery charging power is what is left from the grid power after the losses have been covered.

Finally, by changing the d current component reference to 2 A in a stepwise manner, the transient from V2G into the charging mode is initiated. Fig. 14(a) shows grid-phase voltage v_{ag} , grid current i_{ag} , and battery charging current i_L during this transient. Fast transient response is obvious, although this is not of major concern in this application. From Fig. 14(b), it can be seen that while the d current component follows the reference well, the q -component is kept at zero during the whole transient. As a consequence, the field in the machine pulsates in the same direction. Thus, the machine does not have to be mechanically locked even in transient operation.

It should be noted here that in all experiments resolver readings were taken and these proved that the rotor does not move in

either charging or V2G mode, including the transient. Since such traces have already been shown in [23] and are not particularly visually interesting, they are omitted here. If a PM machine is used instead of the IM, the principle of operation and the control algorithm remain unaltered. The only difference is that the rotor magnetic poles would align with the pulsating filed direction and stay where they are further on during charging process.

C. Propulsion Mode

The operation of configuration of Fig. 1 in the propulsion mode is considered in this section. A reversal transient is performed by changing the speed reference from -800 to 800 r/min. The reference and real speed are shown in Fig. 15, together with the machine's dq current components. It can be seen that the transient is fast, and that the speed tracks its reference well. While the d -component is kept at the constant value, the q -component governs the torque.

Machine phase a current in steady state at speed 800 r/min is shown in Fig. 16. Low-order harmonics are negligibly small, which validates current control described in Section IV-B.

VI. CONCLUSION

This paper proposes a simple multiphase topology that is capable of operating as an on-board integrated battery charger for EVs. The principles can be used with any prime number of phases, greater than three, as discussed in this paper, and are detailed for the five-phase case. A five-phase inverter and a five-phase machine are integrated in the charging process, and fast (three-phase) charging is realized. Electromagnetic torque is not produced in the machine during the charging/V2G mode. Only two additional switches are required to perform hardware reconfiguration between the propulsion and the charging/V2G mode of operation.

This paper explains the idea using the five-phase topology and gives detailed control schemes for the charging and propulsion configurations. Experimental results are provided to validate the torque-free operation with unity power factor, in both charging and V2G modes. Good dynamic behavior in propulsion mode is also demonstrated.

APPENDIX

EXPERIMENTAL RIG DATA

Five-phase induction machine: The equivalent circuit parameters are: $R_s = 2.9 \Omega$, $R_r = 2.2 \Omega$, $L_m = 513$ mH, $L_{\gamma s} = 42.8$ mH, $L_{\gamma r} = 17.4$ mH. The machine has two pole pairs.

DC source/sink: "Spitzenberger & Spies"—two DM 2500/PAS systems connected in series. Power sinking up to 4 kW is enabled by an additional resistive load RL 4000.

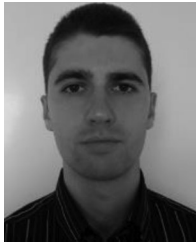
Controller: dSPACE DS1006 processor board. DS2004 high-speed A/D board and DS5101 digital waveform output board are used for the A/D conversion of measured signals and PWM signal generation. Incremental encoder interface board DS3002 is used to validate that machine does not move during the charging/V2G process.

Converter: Custom made eight-phase inverter with EUPEC FS50R12KE3 IGBTs. The continuous rating of five-phases of inverter is approximately 17 kVA.

REFERENCES

- [1] J. M. Slicker, "Pulse width modulation inverter with battery charger," U.S. Patent 4 491 768, Jan. 1, 1985.
- [2] S. Haghbin, S. Lundmark, M. Alakula, and O. Carlson, "Grid-connected integrated battery chargers in vehicle applications: review and new solution," *IEEE Trans. Ind. Electron.*, vol. 60, no. 2, pp. 459–473, Feb. 2013.
- [3] N. Sakr, D. Sadarnac, and A. Gascher, "A review of on-board integrated chargers for electric vehicles," presented at the Eur. Conf. Power Electron. Appl., Lappeenranta, Finland, CD-ROM, 2014.
- [4] M. Yilmaz and P. T. Krein, "Review of battery charger topologies, charging power levels, and infrastructure for plug-in electric and hybrid vehicles," *IEEE Trans. Power Electron.*, vol. 28, no. 5, pp. 2151–2169, May 2013.
- [5] D. Thimmesch, "An SCR inverter with an integral battery charger for electric vehicles," *IEEE Trans. Ind. Appl.*, vol. IA-21, no. 4, pp. 1023–1029, Jul. 1985.
- [6] A. G. Cocconi and W. E. Rippel, "Integrated motor drive and recharge system," U.S. Patent US 5 099 186 A, Mar. 24, 1992.
- [7] A. G. Cocconi, "Combined motor drive and battery recharge system," U.S. Patent US 5 341 075 A, Aug. 23, 1994.
- [8] S. Seung-Ki and L. Sang-Joon, "An integral battery charger for four-wheel drive electric vehicle," *IEEE Trans. Ind. Appl.*, vol. 31, no. 5, pp. 1096–1099, Sep./Oct. 1995.
- [9] L. Solero, "Nonconventional on-board charger for electric vehicle propulsion batteries," *IEEE Trans. Veh. Technol.*, vol. 50, no. 1, pp. 144–149, Jan. 2001.
- [10] L. Jianing, X. Guoqing, J. Linni, and L. Liu, "Electric air conditioner system with on-board charger for PHEV," in *Proc. IEEE Int. Conf. Inf. Autom.*, Shenzhen, China, 2011, pp. 421–426.
- [11] C. Hung-Chun and L. Chang-Ming, "An integrated driving/charging switched reluctance motor drive using three-phase power module," *IEEE Trans. Ind. Electron.*, vol. 58, no. 5, pp. 1763–1775, May 2011.
- [12] J. D. Santiago, H. Bernhoff, B. Ekergerd, S. Eriksson, S. Ferhatovic, R. Waters, and M. Leijon, "Electrical motor drivelines in commercial all-electric vehicles: A review," *IEEE Trans. Veh. Technol.*, vol. 61, no. 2, pp. 475–484, Feb. 2012.
- [13] Renault Press Kit. (2013, Feb. 26). Renault ZOE: The electric supermini for everyday use. [Online]. Available: www.media.renault.com
- [14] C. Saber, "Study and improvement of an integrated charger for electric vehicles' applications," Master MVE Rep. (in French), Arts et Métiers Paris Tech, Lille, France, 2013.
- [15] S. Loudot, B. Briane, O. Ploix, and A. Villeneuve, "Fast charging device for an electric vehicle," U.S. Patent US 2012/0 286 740 A1, Nov. 15, 2012.
- [16] B. Briane and S. Loudot, "Rapid reversible charging device for an electric vehicle," U.S. Patent US 2011/0 254 494 A1, Oct. 20, 2011.
- [17] S. Wall, "Vector control: A practical approach to electric vehicles," in *Proc. IEE Colloq. Vector Control Direct Torque Control Induction Motors*, London, U.K., 1995, IEE Dig. 1995/181, pp. 5/1–5/7.
- [18] J. Hong, H. Lee, and K. Nam, "Charging method for the secondary battery in dual-inverter drive systems for electric vehicles," *IEEE Trans. Power Electron.*, vol. 30, no. 2, pp. 909–921, Feb. 2015.
- [19] L. De Sousa, B. Silvestre, and B. Bouchez, "A combined multiphase electric drive and fast battery charger for electric vehicles," presented at the IEEE Veh. Power Propulsion Conf., Lille, France, 2010.
- [20] A. P. Sandulescu, F. Meinguet, X. Kestelyn, E. Semail, and A. Bruyere, "Flux-weakening operation of open-end winding drive integrating a cost-effective high-power charger," *IET Electr. Syst. Transp.*, vol. 3, no. 1, pp. 10–21, 2013.
- [21] S. Haghbin and I. S. Guillen, "Integrated motor drive and non-isolated battery charger based on the torque cancellation in the motor," presented at the IEEE Int. Conf. Power Electron. Drive Syst., Kitakyushu, Japan, 2013.
- [22] S. Haghbin, K. Khan, Z. Shuang, M. Alakula, S. Lundmark, and O. Carlson, "An integrated 20-kW motor drive and isolated battery charger for plug-in vehicles," *IEEE Trans. Power Electron.*, vol. 28, no. 8, pp. 4013–4029, Jan. 2013.
- [23] I. Subotic, N. Bodo, E. Levi, and M. Jones, "On-board integrated battery charger for EVs using an asymmetrical nine-phase machine," *IEEE Trans. Ind. Electron.*, vol. 62, no. 5, pp. 3285–3295, May 2015.

- [24] I. Subotic, N. Bodo, E. Levi, M. Jones, and V. Levi, "Isolated chargers for EVs incorporating six-phase machines," *IEEE Trans. Ind. Electron.*, doi: 10.1109/TIE.2015.2412516
- [25] E. Levi, M. Jones, S. N. Vukosavic, and H. A. Toliyat, "A novel concept of a multiphase, multimotor vector controlled drive system supplied from a single voltage source inverter," *IEEE Trans. Power Electron.*, vol. 19, no. 2, pp. 320–335, Mar. 2004.
- [26] E. Levi, R. Bojoi, F. Profumo, H. A. Toliyat, and S. Williamson, "Multiphase induction motor drives—A technology status review," *IET Electric Power Appl.*, vol. 1, no. 4, pp. 489–516, 2007.
- [27] M. Jones, S. N. Vukosavic, D. Dujic, and E. Levi, "A synchronous current control scheme for a multiphase induction motor drives," *IEEE Trans. Energy Convers.*, vol. 24, no. 4, pp. 860–868, Dec. 2009.
- [28] H. Guzman, M. J. Duran, F. Barrero, and S. Toral, "Fault-tolerant current predictive control of five-phase induction motor drives with an open phase," in *Proc. IEEE Ind. Electron. Soc. Conf.*, Melbourne, Australia, 2011, pp. 3680–3685.
- [29] C. B. Jacobina, I. S. Freitas, T. M. Oliveira, E. R. C da Silva, and A. M. N. Lima, "Fault tolerant control of five-phase ac motor drive," in *Proc. IEEE Power Electron. Spec. Conf.*, Aachen, Germany, 2004, pp. 3486–3492.
- [30] H. S. Che, E. Levi, M. Jones, W. P. Hew, and N. A. Rahim, "Current control methods for an asymmetrical six-phase induction motor drive," *IEEE Trans. Power Electron.*, vol. 29, no. 1, pp. 407–417, Jan. 2014.



Ivan Subotic (S'12) received the Dipl.Ing. and M.Sc. degrees in electrical engineering from the University of Belgrade, Belgrade, Serbia, in 2010 and 2011, respectively. Since 2011, he has been working toward the Ph.D. degree at the Liverpool John Moores University, Liverpool, U.K.

His main research interests include power electronics, electric vehicles, and control of multiphase drive systems.



Nandor Bodo received the master's degree in 2009 in power electronics from the Faculty of Technical Sciences, University of Novi Sad, Novi Sad, Serbia, and the Ph.D. degree in electrical engineering in 2013 from Liverpool John Moores University, Liverpool, U.K.

He is currently with Liverpool John Moores University as a Postdoctoral Research Associate. His research interests include power electronics and variable speed drives.



Emil Levi (S'89–M'92–SM'99–F'09) received the M.Sc. and Ph.D. degrees in electrical engineering from the University of Belgrade, Yugoslavia, Serbia, in 1986 and 1990, respectively.

From 1982 to 1992, he was with the Department of Electrical Engineering, University of Novi Sad. He joined Liverpool John Moores University, Liverpool, U.K., in May 1992 and since September 2000 is a Professor of electric machines and drives.

Dr. Levi received the Cyril Veinott Award of the IEEE Power and Energy Society in 2009 and the Best Paper Award of the IEEE TRANSACTIONS ON INDUSTRIAL ELECTRONICS in 2008. In 2014, he received the "Outstanding Achievement Award" from the European Power Electronics Association. He served as a Coeditor-in-Chief of the IEEE TRANSACTIONS ON INDUSTRIAL ELECTRONICS from 2009 to 2013, and is currently the Editor-in-Chief of the IET Electric Power Applications and an Editor of the IEEE TRANSACTIONS ON ENERGY CONVERSION.